Construction of a novel platelet-related gene risk model to predict the prognosis and drug response in virus-related hepatocellular carcinoma

JING ZHANG[1], HONGLIN XIANG[2], LING JIANG[1], MEI WANG[1] and GUODONG YANG[1]

[1]Department of Gastroenterology, Affiliated Hospital of North Sichuan Medical College, Nanchong, Sichuan 637000, P.R. China;
[2]Department of Orthopaedics, Laboratory of Biological Tissue Engineering and Digital Medicine, Affiliated Hospital of North Sichuan Medical College, Nanchong, Sichuan 637000, P.R. China

Received May 21, 2024; Accepted September 5, 2024

DOI: 10.3892/ol.2024.14725

Abstract. Platelet activity in the tumor microenvironment (TME) is crucial for the development of tumors. However, the roles and clinical potential of platelet activity in the TME for virus-related hepatocellular carcinoma (HCC) remain unclear. The present study aimed to identify a novel signature based on platelet activity for prognostic prediction and treatment decisions in virus-related HCC. First, a novel platelet signature score (PSS) for each patient with virus-related HCC from The Cancer Genome Atlas was calculated using gene set variation analysis, and the patients were divided into two subgroups (high and low PSS). It was demonstrated that the patients with a high PSS had a worse prognosis, higher platelet activity, stronger inflammation and immunosuppression in TME than patients with a low PSS. Furthermore, 137 differentially expressed genes (DEGs; fold change >2; P<0.05) were identified using 'DESeq2' and 'edgeR' software. Subsequently, 3 genes (cyclin-J-Like protein, nuclear receptor subfamily 0 group B member 1 and tripartite motif containing 54) were identified from DEGs using univariate Cox and least absolute shrinkage and selection operator (LASSO) analyses. Risk score (RS) was calculated based on gene expression and coefficients from LASSO. Patients were divided into high and low RS groups according to the median value, and the 3-gene model was used to predict prognoses and drug responses. Notably, it was demonstrated that patients with a low RS may be better candidates for immune therapy due to lower levels of tumor immune dysfunction and exclusion scores. Moreover, patients with a high RS may be better candidates for nonimmune therapy due to lower half-maximal inhibitory concentration values of drugs (such as AKT inhibitors and gemcitabine). Finally, it was demonstrated that patients with a high PSS and RS had a higher platelet activity, inflammation status, tumor hallmarks and the worst prognosis than patients with a low PSS and RS. This helped to better find patients with these characteristics and suitable treatments using this method. Collectively, the findings of the present study indicate that PSS combined with RS has great potential to evaluate the prognosis of patients with virus -related HCC and assist in deciding treatment strategies.

Correspondence to: Professor Guodong Yang, Department of Gastroenterology, Affiliated Hospital of North Sichuan Medical College, 63 Wenhua Road, Shunqing, Nanchong, Sichuan 637000, P.R. China
E-mail: ygd_ld2003@163.com

Abbreviations: HCC, hepatocellular carcinoma; TME, tumor microenvironment; GSVA, gene set variation analysis; PSS, platelet signature score; TCGA, The Cancer Genome Atlas; RS, risk score; HBV, hepatitis B virus; HCV, hepatitis C virus; ICGC, International Cancer Genome Consortium; GO, Gene Ontology; KEGG, Kyoto Encyclopedia of Genes and Genomes; LASSO, least absolute shrinkage and selection operator; TIDE, The tumor immune dysfunction and exclusion; MSI, microsatellite instability

Key words: virus-related HCC, platelet activity, TME, biomarkers, therapy

Introduction

Primary liver cancer had the sixth highest incidence and the third highest mortality among cancers worldwide in 2020 (1). Hepatocellular carcinoma (HCC) accounts for ~90% of primary liver cancers (2) and the risk factors for HCC include hepatitis B virus (HBV) and hepatitis C virus (HCV) infection, excessive alcohol consumption, nonalcoholic fatty liver disease and exposure to chemical carcinogens such as aflatoxin and aristolochic acids (3). Viral infection remains a leading risk factor for HCC in most Asian countries (4). Hepatitis viruses can promote HCC development in virus carriers through a protumor pathway that differs from that in the nonviral population (5,6). Meanwhile, antiviral therapies can effectively improve the prognosis of patients with virus-related HCC (7,8). Previous studies also reported that virus-related HCC shows unique immune features in its tumor microenvironment (TME) and molecular mechanisms (6,9), which provides a rationale for the development of specific therapeutic targets for virus-related HCC.

Platelets, which are derived from mature megakaryocytes, are characterized by rapid regeneration and no nucleation (10). In addition to limiting blood loss and promoting wound healing, platelets also promote the growth and metastasis of solid tumors, including lung, colon, breast, pancreatic and liver cancers (11). In fact, accumulation of platelets in liver promote liver damage and inflammation in chronic liver diseases through interacting with immune cells (12). In HCC, high platelet counts and platelet activation status are closely associated with poor prognosis (13,14). Limited studies have reported that active platelets may change the TME to support the development of the tumor (15,16). Of note, anti-platelet therapy has been reported to inhibit HCC in a virus-induced HCC mouse model but not in a non-virus-induced HCC mouse model (16). Mechanistically, active platelets accelerate the intrahepatic accumulation of CD8+ T cells to promote carcinogenesis. This finding indicates that platelets may serve a specific role in virus-related HCC.

In addition, the application of bioinformatics technology promotes the development of clinical prognostic models for the treatment and prognosis of patients with HCC (17,18). These models have shown excellent clinical application value and have helped to adjust treatment strategies in patients with HCC (19). However, there is currently no research that has assessed the relationship between platelets and TME based on platelet-related prognostic models in patients with virus-related (HBV and HCV) HCC, to the best of our knowledge. Furthermore, there are no sufficient models to evaluate the association between platelets and the TME in patients with virus-related HCC. Therefore, it is necessary to further explore the underlying hallmarks of virus-related HCC based on platelets to assist in patient classification and clinical prognosis.

The present study constructed a novel platelet signature to identify platelet activation in patients with virus-related HCC. A novel prognostic model based on the difference in platelet activity was then developed to predict the responses to systematic treatments. Finally, the risk score (RS) was combined with the platelet signature score (PSS) to stratify the patients for successful evaluation of platelet activity and tumor hallmarks. Collectively, the present work constructed a novel signature based on platelet activity for prognostic prediction and treatment decision in virus-related HCC.

Materials and methods

Data acquisition. RNA sequencing (RNA-seq) transcriptome data (count and transcript per million values) were obtained from The Cancer Genome Atlas (TCGA) database (TCGA-LIHC; https://portal.gdc.cancer.gov) and assessed using the R package 'TCGAbiolinks' (version 2.24.3). Data from 424 samples were downloaded. Similarly, the clinical information of 377 patients with HCC was obtained through TCGAbiolinks (BiocManager, version 1.30.18). The gene expression of patients with multiple locus samples was replaced by the average of the multiple samples. The genes detected more than twice had the expression value replaced by the average value. A total of 98 patients with virus-related HCC and the corresponding RNA-seq expression profiles were selected according to the following inclusion criteria: i) HBV, HCV or HBV + HVC infection; ii) no risk factors for alcohol, tobacco, non-virus induced cirrhosis and fatty liver disease; and iii) complete clinicopathological information including age, sex, tumor-node-metastasis (TNM) stage (20), survival time and status.

The validation set was obtained from the International Cancer Genome Consortium (ICGC) database (ICGC-LIRI-JP; https://dcc.icgc.org/). The RNA-seq transcriptome data and clinical information of the ICGC-LIRI-JP cohort were downloaded and processed in the same manner as the TCGA data. According to the aforementioned inclusion criteria, 53 patients with virus-related HCC and the corresponding RNA expression profiles were chosen. In addition, 174 patients with HCC with virus infection (HBV, HVC or HBV + HVC) were selected for extended validation of prognosis. The clinical data of the aforementioned patients with virus-related HCC are presented in Tables SI and SII.

Construction of platelet signature and PSS. The specific genes of platelets have been reported in previous experimental studies (21,22). The genes specifically expressed among the top 50 genes in the study by Gnatenko *et al* (21) and genes with a relative expression index >2 in the study by Raghavachari *et al* (22) were combined as the final platelet signature in the present study. The PSS of each sample was calculated using the R package 'GSVA' (version 1.44.5). The patients were then divided into high and low PSS groups according to the cut-off value (0.73) obtained using X-tile software (version 3.6.1; https://x-tile.software.informer.com).

Functional analysis. Platelet-related function and hallmark signatures were obtained from the Molecular Signature Database (M15669; http://www.gsea-msigdb.org/gsea/msigdb/index.jsp) of the Gene Set Enrichment Analysis database (http://www.gsea-msigdb.org/gsea/index.jsp). Subsequently, gene set variation analysis (GSVA) was used to calculate the score of each sample in platelet-related function and hallmark pathways. Gene Ontology (GO) and Kyoto Encyclopedia of Genes and Genomes (KEGG) analyses were performed using the Database for Annotation, Visualization and Integrated Discovery (DAVID) database (https://david.ncifcrf.gov/), and results with $P<0.05$ were considered statistically significant.

Immune analysis. The stromal, immune and tumor purity scores of each sample were obtained using the R package 'ESTIMATE' (version 1.0.13) (23). CIBERSORT (24) and xCell (25) were used to assess the extent of immune cell infiltration. The immune checkpoints were selected based on a previous study (26).

Identification of differentially expressed genes (DEGs) and construction of the protein-protein interaction (PPI) network. DEGs (foldchange >2; $P<0.05$) between the high and low PSS groups were identified using the R packages 'DESeq2' (version 1.36.0) (27) and 'edgeR' (version 3.38.4) (28). Mutual DEGs identified were used as the final DEGs for subsequent analysis. The PPI network was assessed using the Protein-Protein Interaction Networks Functional Enrichment Analysis (STRING) database (https://string-db.org/) and visualized by Cytoscape software (version 3.9.1; https://cytoscape.org/).

Prognostic model construction and evaluation of clinical value. First, univariate Cox analysis of the aforementioned DEGs was used to select the prognostic genes with a significance of P<0.05. Subsequently, least absolute shrinkage and selection operator (LASSO) regression analysis was used to identify the final gene signature according to the minimum λ value (29). The RS of patients with virus-related HCC was evaluated according to the following formula: Risk score=∑ coef (gene) x expr (gene). Patients were then divided into high and low RS groups according to the median value. Based on the RS, Kaplan-Meier analysis was performed and time-dependent receiver operating characteristic (ROC) curves were generated to assess whether the RS could accurately predict the prognosis of patients with virus-related HCC. Furthermore, univariate and multivariate Cox analyses were performed, and a nomogram, calibration curve and ROC curve were generated to evaluate whether the RS can be used as an independent clinical prognostic predictor. Expression and survival of genes for model in HCC was obtained through the University of ALabama at Birmingham CANcer data analysis Portal (UALCAN) database (https://ualcan.pa-th.uab.edu/) and the Human Protein Atlas (HPA) database (https://www.proteinatlas.org/).

Prediction of systemic treatment response. The half-maximal inhibitory concentration (IC_{50}) values of chemotherapy and targeted drugs for patients with virus-related HCC were assessed using the R package 'pRRophetic' (version 0.5). The Tumor Immune Dysfunction and Exclusion (TIDE; http://tide.dfci.harvard.edu/) algorithm (30) was used to predict the anti-programmed cell death protein 1 and anti-cytotoxic T-lymphocyte associated protein 4 (CTLA4) response of each patient with virus-related HCC. Patients whose TIDE scores were <0 were considered non-responders, whilst patients whose TIDE scores were >0 were considered responders. Moreover, microsatellite instability (MSI), dysfunction and exclusion of T cells were also obtained through the TIDE algorithm.

Reverse transcription-quantitative PCR. A total of five paired HBV-related HCC and adjacent tissues from HCC patients who received hepatectomy from May 2019 to June 2019 were collected at the Affiliated Hospital of North Sichuan Medical College (Nanchong, China). The use of samples was approved by Research Ethics Committee of Affiliated Hospital of North Sichuan Medical College (Nanchong, China; approval no. 2023059). Total RNA was extracted using the total RNA isolation kit (cat. no. RE-03011; FOREGENE; Chengdu Fuji Biotechnology Co., Ltd.) from five paired HBV-related HCC and adjacent tissues following the manufacturer's instructions. The primescript™ RT reagent kit (cat. no. RR037A; Takara Biotechnology Co., Ltd.) was used for reverse transcription. The reverse transcription volume was 20 μl and the temperature protocol was 37˚C for 15 min and 85˚C for 5 sec. Subsequently, quantitative PCR was performed using the TB Green® Premix Ex Taq™ II (cat. no. RR820A; Takara Biotechnology Co., Ltd.). The reaction volume was 20 μl and the thermocycling conditions were 95˚C for 30 sec, 95˚C for 5 sec and 60˚C for 30 sec (40 repeats), and a default melt curve procedure. Primer sequences were synthesized by Beijing Tsingke Biotech Co., Ltd. The specific sequences used are as follows: Cyclin-J-like protein (CCNJL), (forward) 5'-CCTGCGCGAGAAGGAACTG-3' and (reverse) 5'-CGTTGTAGCGATCCATGAAGTG-3'; nuclear receptor subfamily 0 group B member 1 (NR0B1), (forward) 5'-CTCACTAGCTCAAAGCAAACGC-3' and (reverse) 5'-GCGCTTGATTTGTGCTCGT-3'; tripartite motif containing 54 (TRIM54), (forward) 5'-AGGAGGTGTGCCAGACTATC-3' and (reverse) 5'-GGTCGCCATACTGACGGATG-3'; GAPDH, (forward) 5'-GGAGCGAGATCCCTCCAAAAT-3' and (reverse) 5'-GGCTGTTGTCATACTTCTCATGG-3'. RNA expression levels were normalized using GAPDH (31).

Statistical analysis. Statistical analyses were performed using R software (version 4.2.1; The R Foundation). Comparisons and pairwise comparisons between two groups were assessed using the Wilcoxon rank-sum test or the Wilcoxon signed-rank test, respectively. Comparisons between ≥3 groups were evaluated using the Kruskal-Wallis test, followed by Dunn's or Steel-Dwass correction.

Comparison of clinical features were assessed using the χ^2 or Fisher's exact test. Kaplan-Meier analysis was used to assess survival using the 'survival' package in R (version 3.4.0) and the cutoff values were obtained using X-tile software (version 3.6.1; https://x-tile.software.informer.com) or the median. DEGs (foldchange >2; P<0.05) between the high and low PSS groups were identified using the 'DESeq2' (version 1.36.0) and 'edgeR' (version 3.38.4) packages obtained by BiocManager (version 1.30.18). Mutual DEGs in DESeq2 and edgeR were used as the final DEGs for subsequent analysis. Correlation analysis was performed using Spearman's correlation analysis. P<0.05 was considered to indicate a statistically significant difference.

Results

High PSS is associated with an unfavorable prognosis. A schematic of the study design is presented in Fig. 1A. First, the transcriptome and clinical profiles of 98 patients with virus-related HCC were obtained from TCGA, as well as the gene set of the platelet signature from previous studies (21,22). A PSS was then calculated for each sample using GSVA. Based on the PSS, X-tile was used to divide patients into high and low PSS groups (Fig. 1B). Kaplan-Meier survival analysis indicated that patients in the high PSS group had a worse prognosis (P=0.026) than patients in the low PSS group (Fig. 1C), indicating that PSS is associated with patient prognosis in virus-related HCC. Notably, no significant difference in platelet counts was demonstrated between the high and low PSS groups (Fig. S1A).

High PSS is associated with stronger platelet activity and inflammation in virus-related HCC. Previous studies reported that platelet count and activation are associated with poor prognosis in patients with HCC (13,14). Furthermore, the accumulation of platelets in the TME promotes HCC progression by accelerating inflammation (16). Therefore, the present study assessed the difference in platelet activity and inflammation in the TME between the high and low PSS groups using GSVA. Notably, it was demonstrated that the main functions of platelets (including activation, aggregation and adhesion) were

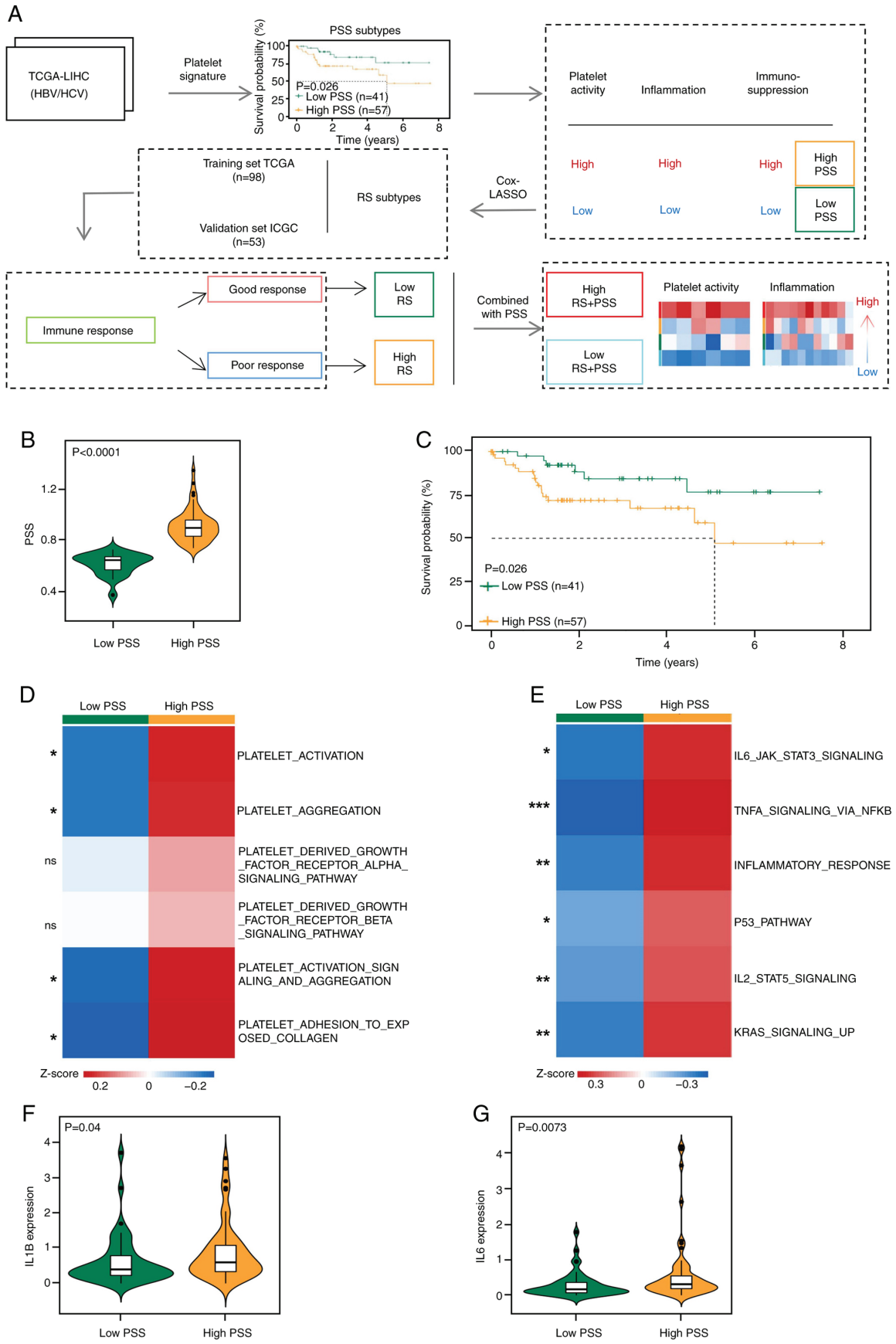

Figure 1. Comparisons between the high and low PSS groups. (A) Schematic of the present study. (B) PSS comparison between the high and low PSS groups. (C) Kaplan-Meier curve showing the prognosis of the high and low PSS groups. The GSVA results revealed the heterogeneity of (D) platelet function and (E) hallmarks in the two subgroups. The color indicates the GSVA enrichment score: Colors from blue to red indicate the GSVA score from low to high. Comparison of (F) IL1B and (G) IL6 expression levels between the high and low PSS groups. *P<0.05; **P<0.01; ***P<0.001. ns, not significant; PSS, platelet signature score; GSVA, gene set variation analysis; LIHC, liver hepatocellular cancer; HBV, hepatitis B virus; HCV, hepatitis C virus; TCGA, The Cancer Genome Atlas; ICGC, International Cancer Genome Consortium; RS, risk score; LASSO, least absolute shrinkage and selection operator.

significantly enriched (P<0.05) in the high PSS group; however, there was no significant difference in the platelet-derived growth factor receptor α or β signaling pathway between the high and low PSS groups (Fig. 1D). Furthermore, GSVA of hallmark pathways indicated that inflammation-related pathways (including IL6-JAK-STAT3, TNF-α via NFκB, inflammatory response and IL2-STAT5 signaling pathways) were significantly enriched (P<0.05) in the high PSS group (Fig. 1E). The P53 and KRAS_UP signaling pathways were also significantly enriched (P<0.05) in the high PSS group, but there was no significant difference in other protumor pathways (including the Wnt-β-catenin, PI3K-AKT-MTOR and MTORC1 signaling pathways) between the high and low PSS groups (Fig. S1E). Subsequently, the expression of several inflammatory factors were compared between the high and low PSS groups. The expression levels of the proinflammatory factors IL1B and IL6 were significantly higher (P=0.04 and P=0.0073, respectively) in the high PSS group than in the low PSS group (Fig. 1F and G). However, the expression levels of IL10, TGFB1 and IFNG were not significantly different between the high and low PSS groups (Fig. S1B-D).

High PSS is associated with stronger immune infiltration and potential immunosuppression. Inflammation, as a double-edged sword in tumor progression, recruits a large number of immune cells to accumulate in the TME to form an inflammatory immune microenvironment (32). Given the high association between inflammation and immunity, the present study assessed the immune infiltration and expression of immune checkpoints in the TME between the high and low PSS groups. First, the ESTIMATE algorithm was used and the results revealed that the high PSS group had significantly higher stromal (P=0.0057) and immune (P=0.024) scores than the low PSS group (Fig. 2A and B). Moreover, the low PSS group had a significantly higher tumor purity (P=0.0056) than the high PSS group (Fig. 2C). To further assess these results, the present study used two algorithms (xCell and CIBERSORT) to evaluate the infiltration of immune cells in the TME in the high and low PSS groups. The xCell results demonstrated that the compositions of activated myeloid dendritic cells, macrophages (including M1 and M2) and neutrophils were significantly higher (P<0.05) in the high PSS group than in the low PSS group. Meanwhile, the high PSS group had significantly lower proportions (P<0.05) of CD4+ central memory T cells, naïve CD8+ T cells, eosinophils, mast cells and B-cell plasma than the low PSS group (Fig. 2D). Similarly, the CIBERSORT results revealed that the high PSS group had significantly higher levels of infiltration (P<0.05) of M2 macrophages and neutrophils than the low PSS group (Fig. S2A). These results indicate that the high PSS group may have infiltration of more immunosuppressive cells than the low PSS group, which contributes to the formation of an immunosuppressive microenvironment. Furthermore, as the expression of immune checkpoints is another crucial factor in the formation of an immunosuppressive microenvironment (33), the present study also compared the mRNA expression levels of 11 immune checkpoints between the high and low PSS groups. The expression levels of Hepatitis A virus cellular receptor 2 (HAVCR2; TIM3), CD80 and CD86 were significantly higher (P<0.05) in the high PSS group than the low PSS group, whilst the expression of other immune checkpoints did not significantly differ between the two groups (Fig. 2E). The aforementioned results suggest that the high PSS group may have a stronger immunosuppressive microenvironment than the low PSS group.

Transcriptomic and functional enrichment analyses between the high and low PSS groups. Intrinsic molecular differences are known to determine the hallmarks of malignant biological behavior in tumor cells (34). Based on the aforementioned results, the present study compared the transcriptome differences between the high and low PSS groups to assess the underlying key molecules and mechanisms. DESeq2 and edgeR (two differentially expressed analysis R packages for sequencing data) were used to identify 137 mutual DEGs between the high and low PSS groups (Fig. 3A). Subsequently, functional enrichment analysis of the 137 DEGs was performed using DAVID to evaluate their functional characteristics. The biological processes results revealed that these DEGs were enriched in cell-cell signaling, chemokine-mediated signaling pathways and inflammatory responses. In molecular function, these DEGs were also enriched in structural molecule activity, receptor binding, CXCR chemokine receptor binding and chemokine activity. Furthermore, the cellular component demonstrated that these DEGs were mainly enriched in extracellular components (Fig. 3B). The results of GO analysis indicated that these DEGs were fully involved in cellular interactions (such as tumor and immune cells) and inflammatory immune responses in the TME. KEGG analysis then revealed that the 137 DEGs were mainly enriched in mineral absorption, *Staphylococcus aureus* infection, pancreatic secretion, the estrogen signaling pathway, the IL-17 signaling pathway and viral protein interactions with cytokines and cytokine receptors (Fig. 3C). Notably, the IL-17 signaling pathway and viral protein interactions with cytokines and cytokine receptors also suggest that these DEGs might serve crucial roles in inflammatory immune responses and virus-related tumoral regulation. In addition, a PPI network was constructed using STRING to show the interactions of 137 DEGs (Fig. 3D).

A novel 3-gene prognostic model based on the RS. Tumoral prognostic models are currently widely used in several clinical and basic studies to identify novel molecular subtypes and aid in clinical prognostic assessment (26). After identifying 137 DEGs, the present study performed univariate Cox analysis for these DEGs. The genes with P<0.05 were then chosen for LASSO regression analysis (Fig. 4A and B), and 3 genes (CCNJL, NR0B1 and TRIM54) were identified to construct the prognostic model. Based on the regression coefficients of the LASSO regression analysis and the expression values of the 3 genes in every sample, an RS was calculated for every patient with virus-related HCC and the median of the RS was used as the cutoff value to divide patients into high and low RS groups (Fig. 4C).

The 3 genes (CCNJL, NR0B1 and TRIM54) were mainly highly expressed in the high RS group (Fig. 4C). Kaplan-Meier survival analysis indicated that the patients with a high RS had a worse prognosis (P=0.0079) than the patients with a low RS (Fig. 4D). Subsequently, a time-dependent ROC curve was used to evaluate the prognostic model and it was demonstrated that

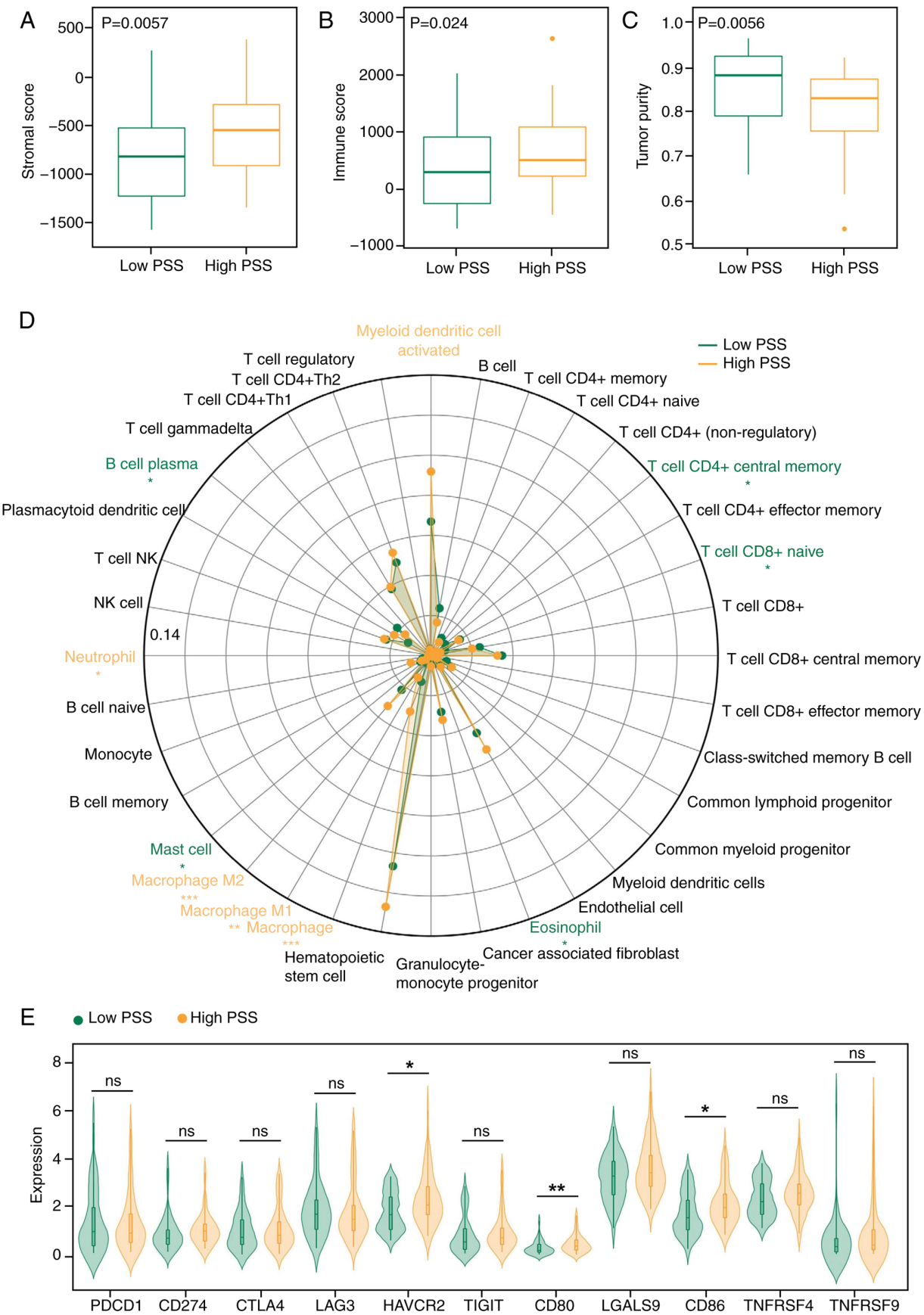

Figure 2. Comparison of the immune microenvironment between the high and low PSS groups. Comparisons of (A) stromal score, (B) immune score and (C) tumor purity between the high and low PSS groups using ESTIMATE. (D) Comparisons of the infiltration of immune cells between the high and low PSS groups using xCell. (E) Comparisons of immune checkpoint expression levels between the high and low PSS groups. *P<0.05; **P<0.01; ***P<0.001. ns, not significant; PSS, platelet signature score; NK, natural killer; PDCD1, programmed cell death protein 1; LAG3, lymphocyte-activation gene 3; TIGIT, T cell immunoreceptor with Ig and ITIM domains; CTLA4, cytotoxic T-lymphocyte associated protein 4; HAVCR2, hepatitis A virus cellular receptor 2; LGALS9, galectin 9, TNFRSF4, TNF receptor superfamily member 4; TNFRSF9, TNF receptor superfamily member 9.

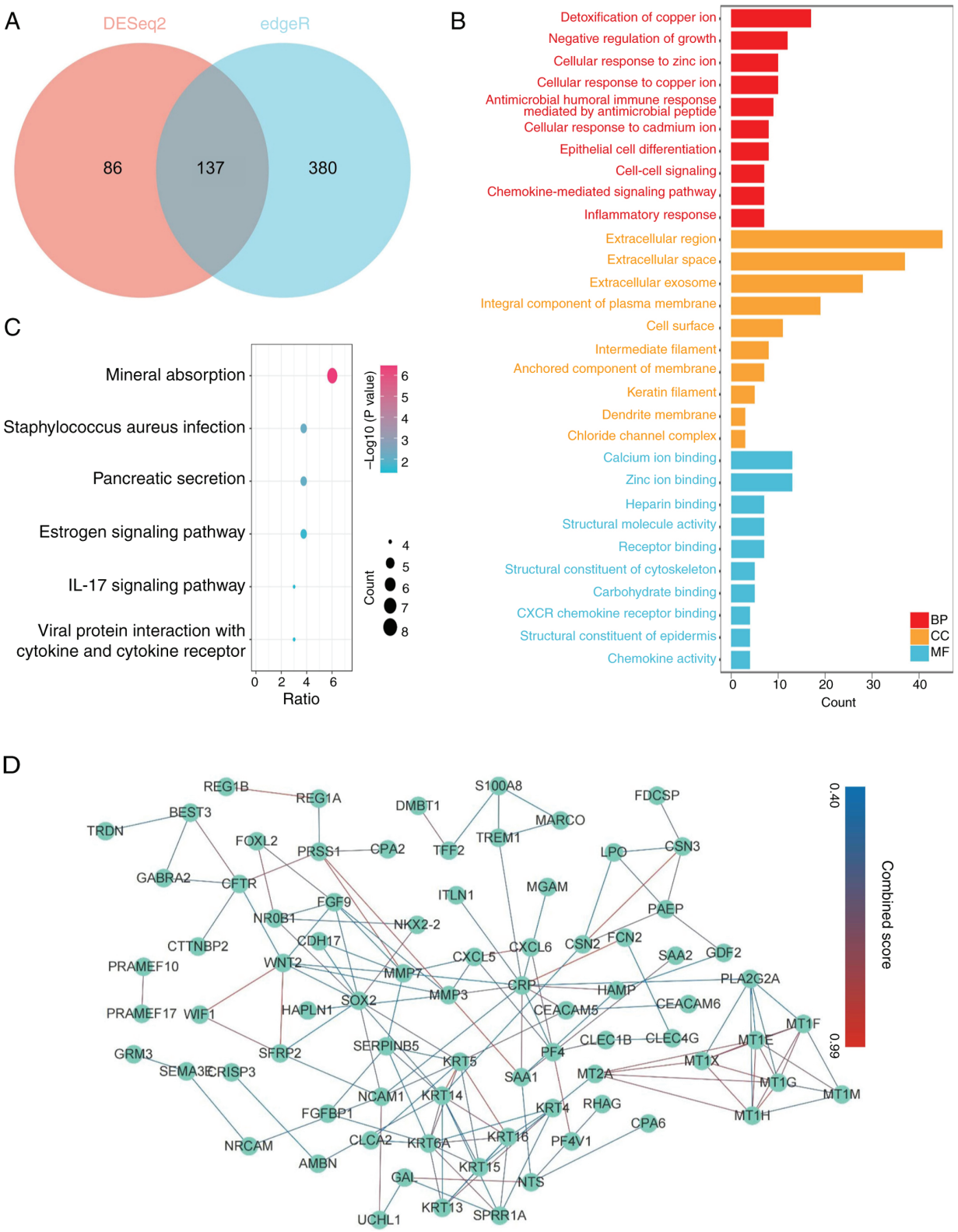

Figure 3. Enrichment analysis of the transcriptome in the high and low PSS groups. (A) Venn diagram showing mutual genes in DESeq2 and edgeR. The mutual genes were considered a subsequent DEG. Results of (B) Gene Ontology and (C) Kyoto Encyclopedia of Genes and Genomes analyses based on the 137 DEGs using DAVID. (D) protein-protein interaction network of 137 DEGs. The green dots represent genes, and the color gradients from yellow to blue represent the combined score of two genes. PSS, platelet signature score; DEG, differentially expressed gene; BP, biological process; CC, cellular component; MF, molecular function.

the area under the curve (AUC) values at 1, 3 and 5 years were 0.80, 0.74 and 0.74, respectively (Fig. 4E). To assess the robustness of the prognostic model, 53 patients with virus-related HCC were chose from the ICGC database. Patients with death or high expression values of the 3 genes were mainly concentrated in the high RS group (Fig. 4F). Kaplan-Meier survival analysis

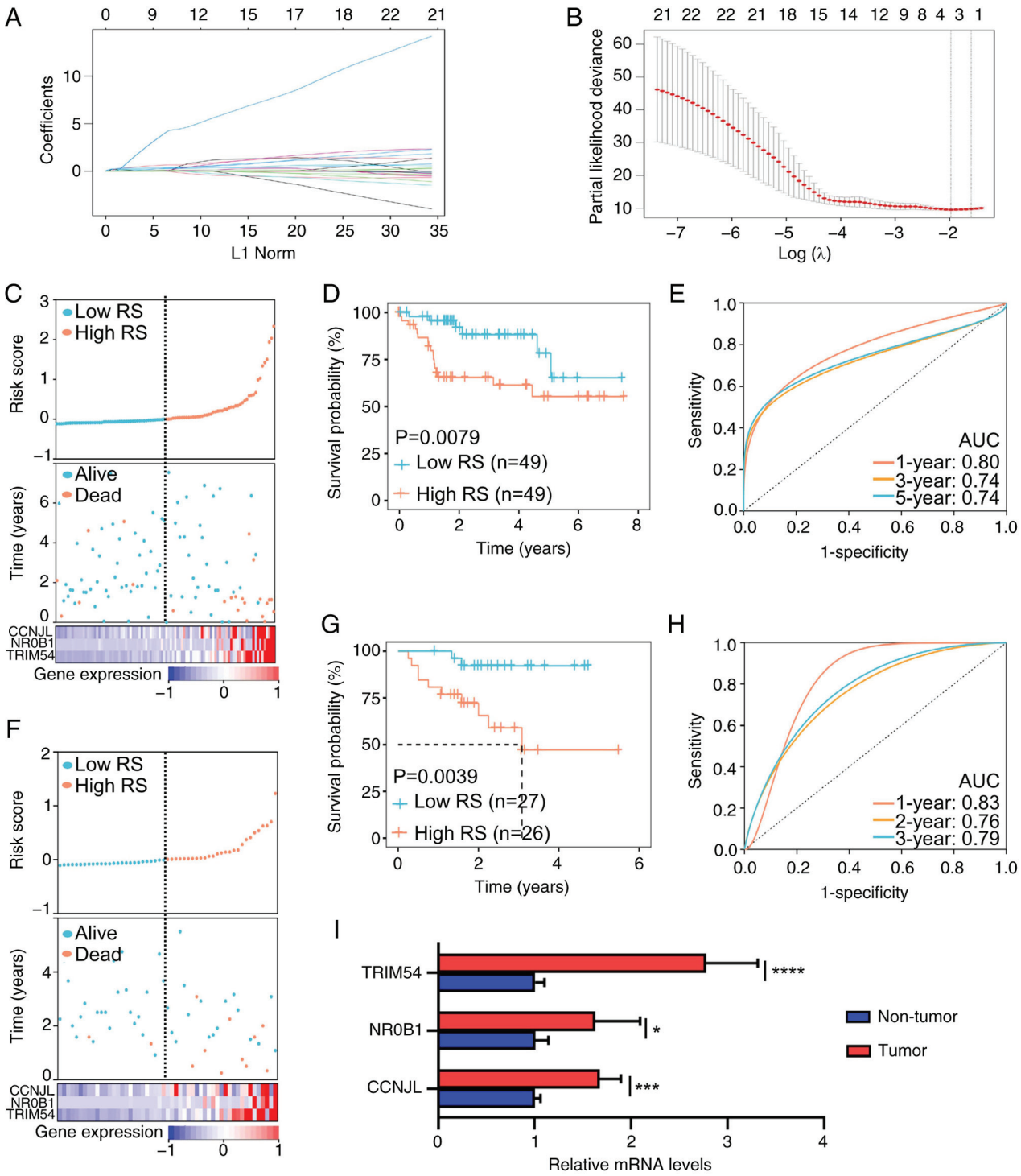

Figure 4. Construction of a 3-gene prognostic model. (A) Least absolute shrinkage and selection operator regression analysis and (B) parameter λ was chosen according to the minimum λ value. (C) Distribution of RS, survival status of patients with virus-related HCC and gene expression patterns of patients in high- and low-risk groups in TCGA. (D) Kaplan-Meier curve showing the prognosis of the high and low RS groups in TCGA. (E) Time-dependent ROC curve showing the AUC values of patients with virus-related HCC at 1, 3 and 5 years in TCGA. (F) Distribution of RS, survival status of patients with virus-related HCC and gene expression patterns of patients in high- and low-risk groups in ICGC. (G) Kaplan-Meier curve showing the prognosis of the high and low RS groups in ICGC. (H) Time-dependent ROC curve showing the AUC values of patients with virus-related HCC at 1, 2 and 3 years in the ICGC. (I) Comparison of mRNA expression levels of the 3 genes (CCNJL, NR0B1 and TRIM54) in HBV-related HCC tissues (n=5). *P<0.05; ***P<0.001; ****P<0.0001. RS, risk score; HCC, hepatocellular carcinoma; TCGA, The Cancer Genome Atlas; ROC, receiver operating characteristic; AUC, area under the curve; ICGC, International Cancer Genome Consortium; CCNJL, cycle-J-like protein; NR0B1, nuclear receptor subfamily 0 group B member 1; TRIM54, tripartite motif containing 54; ns, not significant.

also indicated that the patients with a high RS had a worse prognosis (P=0.0039) than the patients with a low RS (Fig. 4G). Furthermore, the AUC values at 1, 2 and 3 years were 0.83, 0.76 and 0.79, respectively (Fig. 4H). Survival analysis was also performed for 174 patients with HCC with virus infection and other risk factors, and consistent results were obtained (Fig. S3A).

Additionally, the mRNA expression levels of the 3 genes were assessed in 5 paired HBV-related HCC tissues (Fig. 4I), and a Sankey diagram was constructed to show the distribution of patients between the RS and PSS groups (Fig. S3B). Meanwhile, data from the UALCAN database indicated that all 3 genes (CCNJL, NR0B1 and TRIM54) were significantly highly expressed in tumors, and, in comparison with low/medium expression, the high expression of these genes was significantly associated with poor prognosis in patients with HCC (Fig. S3C-H). Considering that genes are not exactly consistent at the mRNA and protein expression levels (35), the present study used the HPA database and revealed that the staining intensity of CCNJL and TRIM54 was notably stronger in tumor tissues than in normal tissues (Fig. S3I and J). Unfortunately, immunohistochemical staining results for NR0B1 could not be obtained from the HPA database.

RS is superior to other common clinical factors in predicting the prognosis of patients with virus-related HCC. After validating the robustness of the model in the present study, the clinical value of the RS was evaluated. First, univariate and multivariate Cox analyses of several clinical factors (including age, sex and TNM staging) and RS were performed. The results of both analyses demonstrated that RS could be an independent prognostic factor for patients with virus-related HCC (Fig. 5A and C). Subsequently, a nomogram was constructed to predict the 1-, 3- and 5-year survival rates of the patients (Fig. 5E). The total score was determined based on individual factor scores and contributed to the survival prediction. Furthermore, the calibration curves were used to describe the accuracy of the model: The calibration curves revealed the highest degree of agreement between the predicted and observed survival probabilities at 3 years in the training set, in comparison with the validation set (Fig. 5G). Notably, the 3-year ROC curves of age, sex, TNM staging and RS demonstrated that RS had the highest AUC value (AUC=0.74; Fig. 5H). Subsequently, the results of Cox analysis from the validation set suggested that RS was a potential independent prognostic factor in virus-related HCC (Fig. 5B and D). The calibration curve also revealed similar results to the training set, and the RS acquired the highest AUC value (AUC=0.79) in the 3-year ROC curves (Fig. 5F, I and J). These results indicate that RS is a potential clinical prognostic indicator in virus-related HCC.

High and low RS groups have different tendencies in systemic therapy. Increasing evidence has demonstrated that patients with HCC benefit from systemic therapy (such as chemotherapy, targeted therapy and immunotherapy), although certain patients are resistant to systemic therapy (36,37). However, there is insufficient evidence to assist in judging the efficacy of systemic therapy in patients with virus-related HCC. The aforementioned results of the present study indicate the importance of RS in prognostic evaluation. Therefore, the potential of RS in predicting the response to systematic treatments was subsequently assessed. First, the IC_{50} of several chemical or targeted drugs indicated that the patients in the high RS group were more likely to be sensitive to chemotherapy and targeted therapy than those in the low RS group. Among these drugs, the IC_{50} values of AKT inhibitor III, gemcitabine, paclitaxel, rapamycin, sorafenib and sunitinib were significantly lower ($P<0.05$) in the high RS group than in the low RS group (Fig. 6A-H). The TIDE, MSI, dysfunction and exclusion scores were then obtained for each sample using the TIDE database. Notably, it was demonstrated that the high RS group had significantly higher TIDE ($P=0.00035$) and exclusion ($P<0.0001$) scores, as well as significantly lower MSI scores ($P=0.016$) than the low RS group, whilst there was no significant difference in the dysfunction score between the high and low RS groups (Fig. 6I-L).

Furthermore, it was demonstrated that the low RS group had a significantly higher response rate to immunotherapy than the high RS group ($P=0.0002$; Fig. 6M). To further support this finding, a correlation analysis was performed between the RS and several immune checkpoints. The results revealed that RS was significantly positively correlated ($P<0.05$) with the expression of CD80, CD86, CTLA4, HAVCR2, galectin 9, TNFRS4 and TNFRS9 (Fig. 6N-T), although there was no significant correlation between RS and the expression of programmed cell death protein 1, CD274, lymphocyte-activation gene 3 and T cell immunoreceptor with Ig and ITIM domains (Fig. S4). Therefore, the results suggest that patients in the high RS group were better suited for chemotherapy or targeted therapy, whilst patients in the low RS group were better suited for immunotherapy.

RS combined with PSS can identify platelet activity, inflammation and protumor pathways in the TME. Given the excellent performance of PSS in predicting platelet activity and inflammation, RS was subsequently combined with PSS to assess the performance in predicting platelet activity, inflammation and pro-tumor pathways. The high RS combined with high PSS group had significantly higher scores for platelet activation, platelet aggregation, platelet-derived growth factor receptor β signaling pathway and platelet activation signaling and aggregation ($P<0.05$) than the low RS combined with low PSS group (Fig. 7A). These results indicated that the high RS combined with high PSS group may have the highest platelet activity among the four groups. Compared with the low RS combined with low PSS group, it was demonstrated that inflammatory-related pathways (including IL6-JAK-STAT3, TNFA via NFκB, inflammatory response and the IL2-STAT5 signaling pathways) were significantly enriched ($P<0.05$) in the high RS combined with high PSS group, which was consistent with previous results based on the PSS. Notable, it was also demonstrated that tumor-related pathways (including the PI3K-AKT-MTOR, MTORC1 and P53 signaling pathways and genes up-regulated by KRAS activation) were significantly enriched ($P<0.05$) in the high RS combined with high PSS group, which was not demonstrated in the separate PSS groupings (Figs. 7B-D and S5A-I). Notably, mutated P53 exerts oncogenic effects through other tumor-related pathways and activates downstream feedback to inhibit the death of tumor cells (38).

Furthermore, it was demonstrated that the high RS combined with high PSS group had a significantly higher ($P<0.05$) expression of inflammatory factors including IL1B, IFNG, TGFB1 and IL10 than the low RS combined with low PSS group (Figs. 7E and F and S5J-L). Additionally, Kaplan-Meier survival analysis indicated that the high RS combined with high PSS group had the worst prognosis ($P=0.002$) among

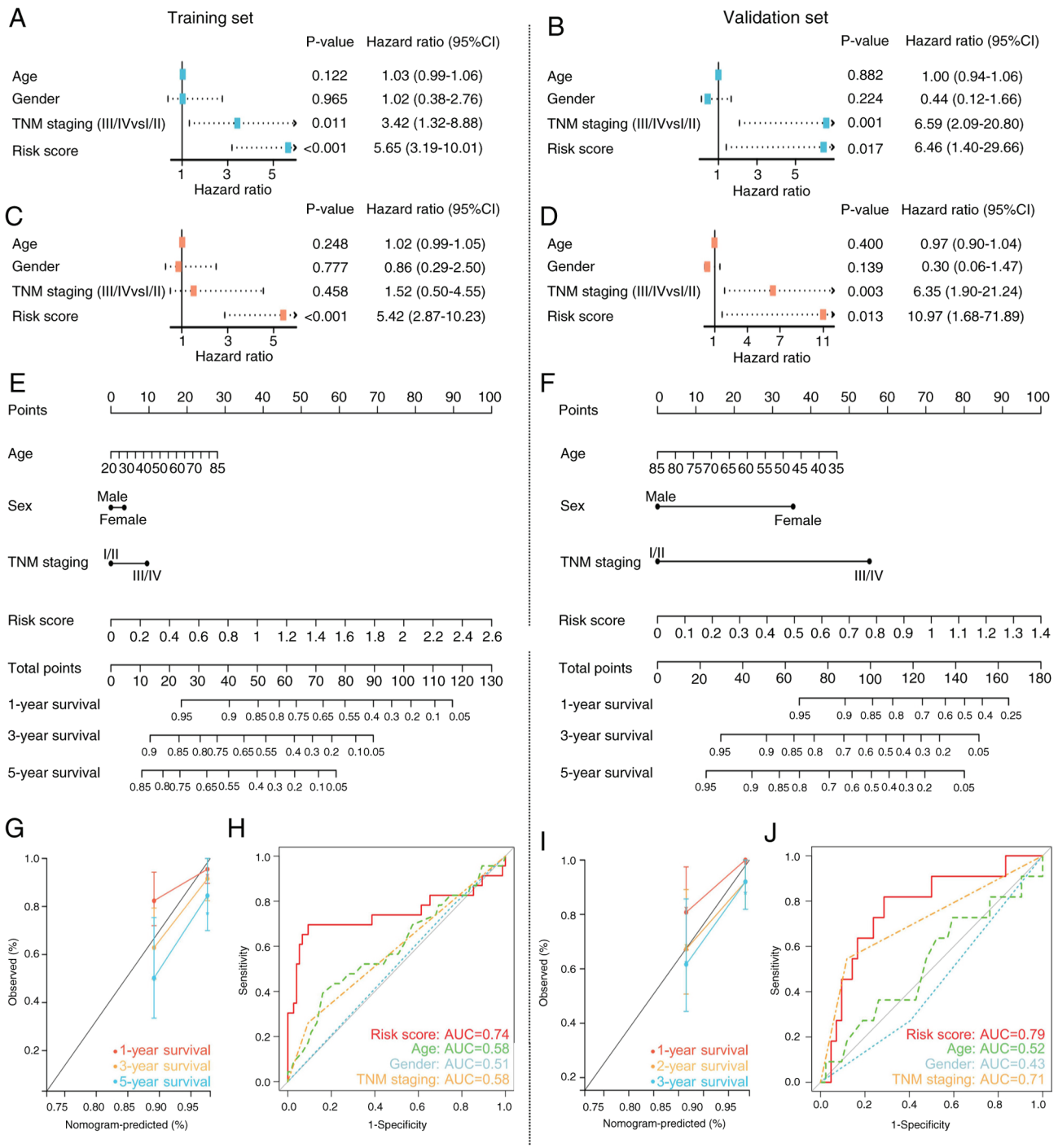

Figure 5. Assessment of the clinical potential of risk score. (A) Univariate and (B) multivariate Cox analyses in TCGA. (C) Nomogram and (D) calibration curve at 1, 3 and 5 years in TCGA. (E) ROC curves show the AUC values of risk score and other clinical features at 3 years in the TCGA. (F) Univariate and (G) multivariate Cox analyses in ICGC. (H) Nomogram and (I) calibration curve at 1, 2 and 3 years in ICGC. (J) ROC curves show the AUC values of risk score and other clinical features at 3 years in the ICGC. TCGA, The Cancer Genome Atlas; AUC, area under the curve; ROC, receiver operating characteristic; ICGC, International Cancer Genome Consortium; TNM, tumor-node-metastasis; CI, confidence interval.

the four groups (Fig. 7G). In summary, these results indicate that RS combined with PSS could predict platelet activity, inflammation and protumor pathways in the TME.

Discussion

An imbalanced inflammatory response is important for the development of HCC (39). Meanwhile, viral infection activates the immune response and aggravates imbalanced inflammation in the liver (4). Furthermore, an experimental study reported that active platelets could recruit virus-specific T cells to the liver and that antiplatelet therapies effectively inhibited the development of virus-related HCC (16). Due to these findings, the present study assessed the role of platelets in virus-related HCC and the regulatory relationship between platelet function and inflammation in the TME. The results of the present study indicate that high platelet activity contributes to poor prognosis, inflammation and immune infiltration in patients

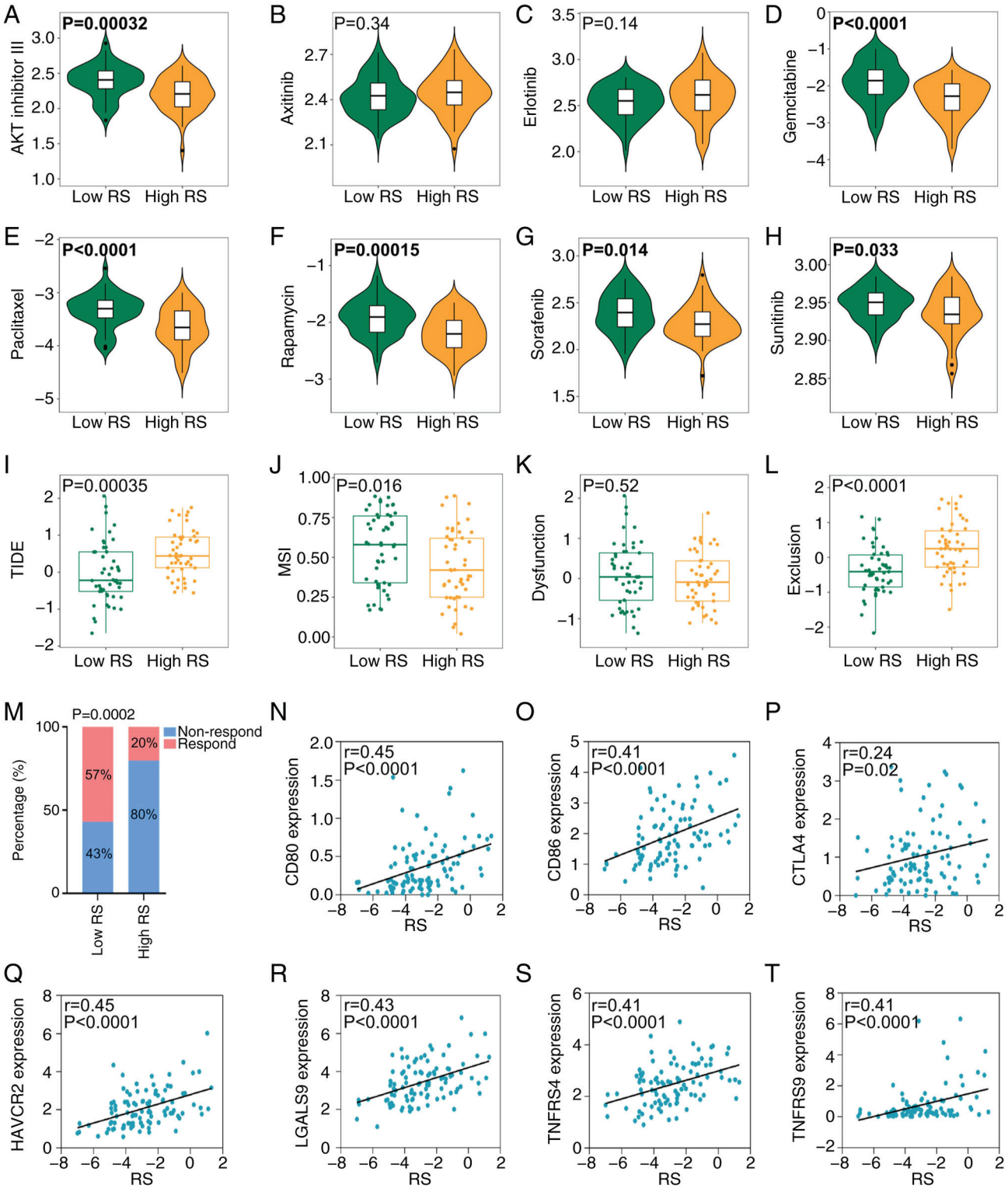

Figure 6. Comparisons of systemic therapy between the high and low RS groups in The Cancer Genome Atlas. Comparisons of nonimmune drug half-maximal inhibitory concentration values between the high and low RS groups: (A) AKT inhibitor III, (B) axitinib, (C) erlotinib, (D) gemcitabine, (E) paclitaxel, (F) rapamycin, (G) sorafenib and (H) sunitinib. Comparisons of (I) TIDE, (J) MSI, (K) dysfunction and (L) exclusion between the high and low RS groups. (M) Comparison of response rates to immunotherapy between the high and low RS groups. Spearman analysis showed a linear relationship between RS and the mRNA expression levels of immune checkpoints: (N) CD80, (O) CD86, (P) CTLA4, (Q) HAVCR2, (R) LGALS9, (S) TNFRS4 and (T) TNFRS9. RS, risk score; TIDE, tumor immune dysfunction and exclusion; MSI, microsatellite instability; CTLA4, cytotoxic T-lymphocyte associated protein 4; HAVCR2, hepatitis A virus cellular receptor 2; LGALS9, galectin 9; ns, not significant.

with virus-related HCC. Moreover, a novel prognostic model was constructed based on platelet activity, which successfully predicted patient responses to several drugs. This provides a novel perspective for individualized targeted therapies in patients with virus-related HCC. Furthermore, the results indicate that PSS combined with RS could identify patients with

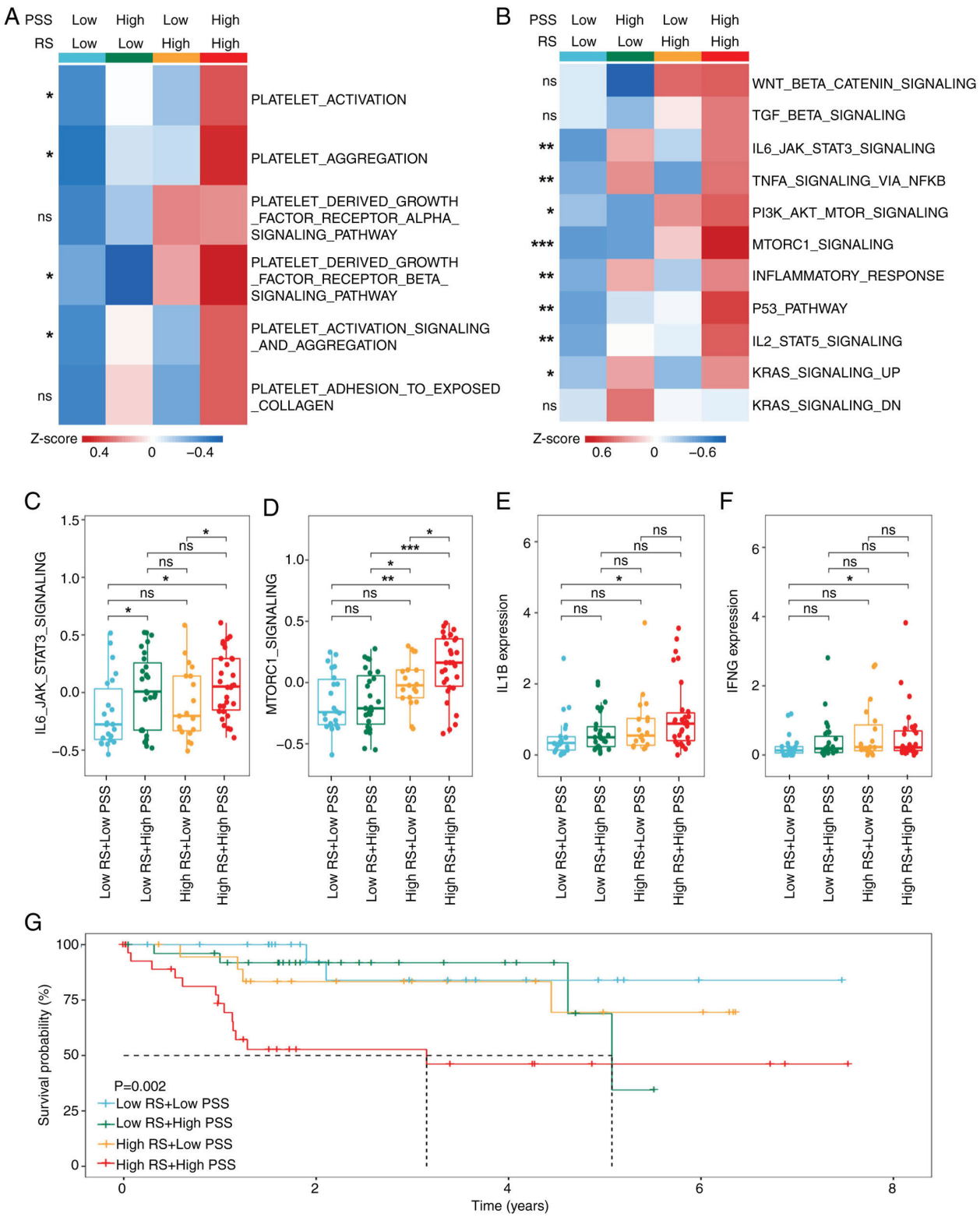

Figure 7. Heterogeneity of platelet function, inflammation and malignancy among the four groups of patients with virus-related hepatocellular carcinoma from TCGA. The GSVA results demonstrated the heterogeneity of (A) platelet function and (B) hallmarks in the four subgroups. The color indicates the GSVA enrichment score: Colors from blue to red indicate the GSVA score from low to high. Comparisons of representative (C) inflammation-related pathways, (D) malignancy-related pathways, (E) IL1B and (F) IFNG expression among the four groups. (G) Kaplan-Meier curve showing the prognosis of the four groups in TCGA. *P<0.05; **P<0.01; ***P<0.001. TCGA, The Cancer Genome Atlas; GSVA, gene set variation analysis; RS, risk score; PSS, platelet signature score; ns, not significant.

poor prognosis, high platelet activity and tumor hallmarks, which could further guide the subsequent clinical treatment selection (immune or non-immune therapies).

The present study revealed that high platelet activity indicates an active inflammatory reaction, which leads to a poor prognosis in patients with virus-related HCC. In addition,

infiltrated immune cells involved in inflammation also serve important roles in promoting or fighting cancer (40), which greatly increases the complexity of the regulatory relationship between inflammation and immunity in the TME. The present study demonstrated that patients with virus-related HCC with active inflammation had more immune cells infiltrating the TME. Notably, active inflammation and platelet activity in the TME may indicate inhibitory immune function in patients with virus-related HCC. Previous studies reported that active platelets and suppressed immune function were the two crucial protumor factors that cause poor prognosis in patients with virus-related HCC (14,26), which is consistent with the poor prognosis of patients with virus-related HCC in the present study. Therefore, we hypothesize that platelet activity, inflammation and immunity suppression in the TME synergistically promotes the development of virus-related HCC. Furthermore, the present study revealed that the infiltration of macrophages and T cells in the TME was different between the high and low PSS groups in addition to, which indicates that active platelets may regulate inflammation and the immune response via macrophages to ultimately promote virus-related HCC. Notably, the association between platelets and macrophages has been previously reported in a chemically induced animal model of HCC (15). Therefore, macrophages may be a potential candidate for targeted therapy. Exploring the keys to platelet regulation of macrophages may be beneficial for subsequent reversal of the overall protumor effect of macrophages in virus-related HCC.

Tolerance to drug therapies remains a formidable challenge in the treatment of patients with HCC (41,42). Imbalanced inflammation and immune suppression are two crucial factors in resistance to drugs (41). For patients with virus-related HCC, there are still no effective biomarkers to predict the response to targeted drugs. The present study revealed that patients with virus-related HCC with a low RS were more likely to benefit from immunotherapy (such as immune checkpoint inhibitors), whilst patients with a high RS were more likely to benefit from non-immunotherapy (such as sorafenib). The present work illustrates the necessity and potential clinical benefits of precisely targeted therapies in patients with virus-related HCC from the perspective of platelet activity. Furthermore, the present study also identified a special subtype with high platelet activity, inflammation and malignancy in patients with virus-related HCC. Notably, patients in this subtype had the worst prognosis among the four subtypes, which was consistent with the indication that high platelet activity and inflammation demonstrated immune suppression in the TME and poor prognosis in patients with virus-related HCC. Therefore, patients in this subtype should be the key population for follow-up treatment and exploration in virus-related HCC.

However, there are still several limitations in the present study. First, the present study was mainly based on public databases and lacks cohort validation of more sample clinical samples as well as prospective studies. Second, the present study lacks basic experimental and mechanistic studies concerning several specific molecules. Nevertheless, the results of the present study deepen the understanding of platelet activity in virus-related HCC. Moreover, the novel model based on integrated prognostic and functional approaches contributes to the evaluation of patient prognosis and drug response. However, subsequent work needs to be performed, with more clinical samples to further verify the model based on the clinical data in the present study. Furthermore, the exploration and verification of the molecular mechanisms by which platelets regulate inflammation and immune infiltration in patients with virus-related HCC is required. In addition, there is a need to focus on different features of platelets between HBV- and HCV-related HCC as well as mutual features.

In summary, the present study constructed and validated a 3-gene signature prognostic model based on the platelet activity in TME of patients with virus-related HCC. In addition, the present study validated the expression of 3 genes in HCC tissues. Furthermore, the model used in the present study could evaluate platelet activity and therapeutic response. Therefore, the present work provides novel insights for prognostic prediction and individualized treatment of patients with virus-related HCC from the perspective of platelets.

Acknowledgements

Not applicable.

Funding

No funding was received.

Availability of data and materials

The data generated in the present study may be requested from the corresponding author.

Authors' contributions

JZ, HX, LJ, MW and GY contributed to the study conception and design. Material preparation, data collection and analysis were performed by JZ, HX and LJ. The literature search was performed by LJ and MW. The first draft of the manuscript was written by JZ and the final revision of the manuscript was performed by GY. JZ and GY confirm the authenticity of all the raw data. All authors have read and approved the final manuscript.

Ethics approval and consent to participate

The present study was approved by the Research Ethics Committee of the Affiliated Hospital of North Sichuan Medical College (Nanchong, China; approval no. 2023059). The confidentiality of patient information was maintained using a de-identified and anonymous manner. Written informed consent was obtained from all participants.

Patient consent for publication

Not applicable.

Competing interests

The authors declare that they have no competing interests.

References

1. Sung H, Ferlay J, Siegel RL, Laversanne M, Soerjomataram I, Jemal A and Bray F: Global cancer statistics 2020: GLOBOCAN estimates of incidence and mortality worldwide for 36 cancers in 185 countries. CA Cancer J Clin 71: 209-249, 2021.
2. Llovet JM, Kelley RK, Villanueva A, Singal AG, Pikarsky E, Roayaie S, Lencioni R, Koike K, Zucman-Rossi J and Finn RS: Hepatocellular carcinoma. Nat Rev Dis Primers 7: 6, 2021.
3. Villanueva A: Hepatocellular carcinoma. N Engl J Med 380: 1450-1462, 2019.
4. Zhang CH, Cheng Y, Zhang S, Fan J and Gao Q: Changing epidemiology of hepatocellular carcinoma in Asia. Liver Int 42: 2029-2041, 2022.
5. Lim CJ, Lee YH, Pan L, Lai L, Chua C, Wasser M, Lim TKH, Yeong J, Toh HC, Lee SY, *et al*: Multidimensional analyses reveal distinct immune microenvironment in hepatitis B virus-related hepatocellular carcinoma. Gut 68: 916-927, 2019.
6. Song G, Shi Y, Zhang M, Goswami S, Afridi S, Meng L, Ma J, Chen Y, Lin Y, Zhang J, *et al*: Global immune characterization of HBV/HCV-related hepatocellular carcinoma identifies macrophage and T-cell subsets associated with disease progression. Cell Discov 6: 90, 2020.
7. Zhang S, Gao S, Zhao M, Liu Y, Bu Y, Jiang Q, Zhao Q, Ye L and Zhang X: Anti-HBV drugs suppress the growth of HBV-related hepatoma cells via down-regulation of hepatitis B virus X protein. Cancer Lett 392: 94-104, 2017.
8. Yeh ML, Liang PC, Tsai PC, Wang SC, Leong J, Ogawa E, Jun DW, Tseng CH, Landis C, Tanaka Y, *et al*: Characteristics and survival outcomes of hepatocellular carcinoma developed after HCV SVR. Cancers (Basel) 13: 3455, 2021.
9. Wang SH, Yeh SH and Chen PJ: Unique features of hepatitis B virus-related hepatocellular carcinoma in pathogenesis and clinical significance. Cancers (Basel) 13: 2454, 2021.
10. Holinstat M: Normal platelet function. Cancer metastasis Rev 36: 195-198, 2017.
11. Haemmerle M, Stone RL, Menter DG, Afshar-Kharghan V and Sood AK: The platelet lifeline to cancer: Challenges and opportunities. Cancer Cell 33: 965-983, 2018.
12. Ramadori P, Klag T, Malek NP and Heikenwalder M: Platelets in chronic liver disease, from bench to bedside. JHEP Rep 1: 448-459, 2019.
13. Scheiner B, Kirstein M, Popp S, Hucke F, Bota S, Rohr-Udilova N, Reiberger T, Müller C, Trauner M, Peck-Radosavljevic M, *et al*: Association of platelet count and mean platelet volume with overall survival in patients with cirrhosis and unresectable hepatocellular carcinoma. Liver Cancer 8: 203-217, 2019.
14. Wang B, Zhu J, Ma X, Wang H, Qiu S, Pan B, Zhou J, Fan J, Yang X, Guo W and Cheng Y: Platelet activation status in the diagnosis and postoperative prognosis of hepatocellular carcinoma. Clin Chim Acta 495: 191-197, 2019.
15. Pavlović N, Kopsida M, Gerwins P and Heindryckx F: Activated platelets contribute to the progression of hepatocellular carcinoma by altering the tumor environment. Life Sci 277: 119612, 2021.
16. Sitia G, Iannacone M and Guidotti LG: Anti-platelet therapy in the prevention of hepatitis B virus-associated hepatocellular carcinoma. J Hepatol 59: 1135-1138, 2013.
17. Long J, Wang A, Bai Y, Lin J, Yang X, Wang D, Yang X, Jiang Y and Zhao H: Development and validation of a TP53-associated immune prognostic model for hepatocellular carcinoma. EBioMedicine 42: 363-374, 2019.
18. Tang B, Zhu J, Zhao Z, Lu C, Liu S, Fang S, Zheng L, Zhang N, Chen M, Xu M, *et al*: Diagnosis and prognosis models for hepatocellular carcinoma patient's management based on tumor mutation burden. J Adv Res 33: 153-165, 2021.
19. Calderaro J, Seraphin TP, Luedde T and Simon TG: Artificial intelligence for the prevention and clinical management of hepatocellular carcinoma. J Hepatol 76: 1348-1361, 2022.
20. Edge SB, Byrd DR, Compton CC, Fritz AG, Greene FL and Trott A: AJCC Cancer Staging Manual. Edge SB (ed). 7th edition. Springer, New York, NY, pp191-201, 2010.
21. Gnatenko DV, Dunn JJ, McCorkle SR, Weissmann D, Perrotta PL and Bahou WF: Transcript profiling of human platelets using microarray and serial analysis of gene expression. Blood 101: 2285-2293, 2003.
22. Raghavachari N, Xu X, Harris A, Villagra J, Logun C, Barb J, Solomon MA, Suffredini AF, Danner RL, Kato G, *et al*: Amplified expression profiling of platelet transcriptome reveals changes in arginine metabolic pathways in patients with sickle cell disease. Circulation 115: 1551-1562, 2007.
23. Yoshihara K, Shahmoradgoli M, Martínez E, Vegesna R, Kim H, Torres-Garcia W, Treviño V, Shen H, Laird PW, Levine DA, *et al*: Inferring tumour purity and stromal and immune cell admixture from expression data. Nat Commun 4: 2612, 2013.
24. Newman AM, Liu CL, Green MR, Gentles AJ, Feng W, Xu Y, Hoang CD, Diehn M and Alizadeh AA: Robust enumeration of cell subsets from tissue expression profiles. Nat Methods 12: 453-457, 2015.
25. Aran D, Hu Z and Butte AJ: xCell: digitally portraying the tissue cellular heterogeneity landscape. Genome Biol 18: 220, 2017.
26. Xie H, Shi M, Liu Y, Cheng C, Song L, Ding Z, Jin H, Cui X, Wang Y, Yao D, *et al*: Identification of m6A- and ferroptosis-related lncRNA signature for predicting immune efficacy in hepatocellular carcinoma. Front Immunol 13: 914977, 2022.
27. Love MI, Huber W and Anders S: Moderated estimation of fold change and dispersion for RNA-seq data with DESeq2. Genome Biol 15: 550, 2014.
28. Robinson MD, McCarthy DJ and Smyth GK: edgeR: A Bioconductor package for differential expression analysis of digital gene expression data. Bioinformatics 26: 139-140, 2010.
29. Liang JY, Wang DS, Lin HC, Chen XX, Yang H, Zheng Y and Li YH: A novel ferroptosis-related gene signature for overall survival prediction in patients with hepatocellular carcinoma. Int J Biol Sci 16: 2430-2441, 2020.
30. Jiang P, Gu S, Pan D, Fu J, Sahu A, Hu X, Li Z, Traugh N, Bu X, Li B, *et al*: Signatures of T cell dysfunction and exclusion predict cancer immunotherapy response. Nat Med 24: 1550-1558, 2018.
31. Fang Z, Sun X, Wang X, Ma J, Palaia T, Rana U, Miao B, Ragolia L, Hu D and Miao QR: NOGOB receptor deficiency increases cerebrovascular permeability and hemorrhage via impairing histone acetylation-mediated CCM1/2 expression. J Clin Invest 132: e151382, 2022.
32. Mantovani A, Allavena P, Sica A and Balkwill F: Cancer-related inflammation. Nature 454: 436-444, 2008.
33. Cocco C, Morandi F and Airoldi I: Immune checkpoints in pediatric solid tumors: Targetable pathways for advanced therapeutic purposes. Cells 10: 927, 2021.
34. Rebouissou S and Nault JC: Advances in molecular classification and precision oncology in hepatocellular carcinoma. J Hepatol 72: 215-229, 2020.
35. Liu Y, Beyer A and Aebersold R: On the dependency of cellular protein levels on mrna abundance. Cell 165: 535-550, 2016.
36. Llovet JM, Montal R, Sia D and Finn RS: Molecular therapies and precision medicine for hepatocellular carcinoma. Nat Rev Clin Oncol 15: 599-616, 2018.
37. Sonbol MB, Riaz IB, Naqvi SAA, Almquist DR, Mina S, Almasri J, Shah S, Almader-Douglas D, Uson Junior PLS, Mahipal A, *et al*: Systemic therapy and sequencing options in advanced hepatocellular carcinoma: A systematic review and network meta-analysis. JAMA Oncol 6: e204930, 2020.
38. Liu Y and Gu W: The complexity of p53-mediated metabolic regulation in tumor suppression. Semin Cancer Biol 85: 4-32, 2022.
39. Ringelhan M, Pfister D, O'Connor T, Pikarsky E and Heikenwalder M: The immunology of hepatocellular carcinoma. Nat Immunol 19: 222-232, 2018.
40. Keenan BP, Fong L and Kelley RK: Immunotherapy in hepatocellular carcinoma: The complex interface between inflammation, fibrosis, and the immune response. J Immunother Cancer 7: 267, 2019.
41. Syn NL, Teng MWL, Mok TSK and Soo RA: De-novo and acquired resistance to immune checkpoint targeting. Lancet Oncol 18: e731-e741, 2017.
42. Tang W, Chen Z, Zhang W, Cheng Y, Zhang B, Wu F, Wang Q, Wang S, Rong D, Reiter FP, *et al*: The mechanisms of sorafenib resistance in hepatocellular carcinoma: theoretical basis and therapeutic aspects. Signal Transduct Target Ther 5: 87, 2020.